

# Unconditionally Long-Time Stable Variable-Step Second-Order Exponential Time-Differencing Schemes for the Incompressible NSE

Haifeng Wang<sup>a</sup>, Xiaoming Wang<sup>a,\*</sup>, Min Zhang<sup>b,a</sup>

<sup>a</sup>*School of Mathematical Sciences, Eastern Institute of Technology, Zhejiang, Ningbo, 315200, China*

<sup>b</sup>*School of Mathematical Sciences, Shanghai Jiao Tong University, Shanghai, 200240, China*

---

## Abstract

We develop an efficient, unconditionally stable, variable-step second-order exponential time-differencing (ETD) scheme for the incompressible Navier–Stokes equations in two and three spatial dimensions under periodic boundary conditions, together with an embedded adaptive time-stepping variant. The scheme is unconditionally uniform-in-time stable in the sense that the numerical solution admits a time-uniform bound in  $L^\infty(0, \infty; (L^2)^d)$  whenever the external forcing term is uniformly bounded in time in  $L^2$ , for all Reynolds numbers and for arbitrary choices of time step sizes.

At each time step, the method requires the solution of two time-dependent Stokes problems, which can be evaluated explicitly in the periodic setting using Fourier techniques, along with the solution of a single scalar cubic algebraic equation. Beyond the standard ETD framework, the proposed scheme incorporate two recently developed ingredients: (i) a dynamic second-order scalar auxiliary variable (SAV) correction, which is essential for achieving second-order temporal accuracy, and (ii) a mean-reverting scalar auxiliary variable (mr-SAV) multistep formulation, which plays a central role in ensuring long-time stability.

The proposed methods overcome key limitations of existing approaches for the Navier–Stokes equations: classical Runge–Kutta schemes generally lack provable long-time stability, while IMEX and SAV-based BDF methods typically do not admit unconditional stability guarantees in the variable-step setting. Numerical experiments in two spatial dimensions confirm second-order temporal accuracy, uniform long-time stability, and effective error control provided by the adaptive strategy. Rigorous convergence analysis and a systematic investigation of long-time statistical properties will be pursued in future work.

*Keywords:* incompressible Navier-Stokes equation, exponential time-differencing (ETD), mean reverting scalar auxiliary variable (mr-SAV), unconditional stability, long time stability, second-order time marching, variable step, time-adaptive scheme

*2020 MSC:* 65M12, 65L04, 65L05, 76D05

---

## 1. Introduction

The incompressible Navier–Stokes equations (NSE) constitute a fundamental mathematical model for viscous incompressible fluid flows and arise in a wide range of scientific and engineering applications, including geophysical flows, atmospheric and oceanic dynamics, turbulence, and climate science. In this paper, we consider the NSE

$$\frac{\partial \mathbf{u}}{\partial t} + \mathbf{u} \cdot \nabla \mathbf{u} = \nu \Delta \mathbf{u} - \nabla p + \mathbf{f}, \quad (1.1a)$$

$$\nabla \cdot \mathbf{u} = 0, \quad (1.1b)$$

posed on a rectangular domain  $\Omega \subset \mathbb{R}^d$  ( $d = 2, 3$ ) equipped with periodic boundary conditions. To ensure uniqueness and stability, we impose zero-mean conditions on the velocity field  $\mathbf{u} = (u_1, \dots, u_d)$ , the pressure  $p$ , and the external forcing  $\mathbf{f}$ . Here,  $\nu > 0$  denotes the kinematic viscosity, and  $\mathbf{f}$  represents an external body force that is assumed to be uniformly bounded in time. The periodic boundary condition enables us to eliminate the pressure by applying the classical Leray–Hopf projection, which can be calculated explicitly and efficiently in Fourier space.

In two spatial dimensions, the periodic NSE can equivalently be written in the vorticity–streamfunction formulation

$$\begin{aligned} \omega_t + \mathbf{u} \cdot \nabla \omega &= \nu \Delta \omega + f, \\ \Delta \psi &= \omega, \quad \mathbf{u} = \nabla^\perp \psi := (\partial_y \psi, -\partial_x \psi), \end{aligned} \quad (1.2)$$

where  $\omega = \nabla \times \mathbf{u}$  denotes the scalar vorticity,  $\psi$  is the streamfunction, and  $f = \nabla^\perp \cdot \mathbf{f}$  is the forcing term in this formulation. The incompressibility constraint is automatically

---

\*Corresponding author

Email addresses: [hfwang@eitech.edu.cn](mailto:hfwang@eitech.edu.cn) (Haifeng Wang), [wxm@eitech.edu.cn](mailto:wxm@eitech.edu.cn) (Xiaoming Wang ), [zhangmm@sjtu.edu.cn](mailto:zhangmm@sjtu.edu.cn) (Min Zhang)

satisfied, and the pressure variable is eliminated, making this formulation particularly attractive for numerical simulations in periodic domains.

A fundamental qualitative property of the NSE is the *uniform-in-time boundedness* of solutions in the energy norm. In particular, when the external forcing is uniformly bounded in  $L^2$ , the velocity field admits a global-in-time  $L^2$  bound, independent of whether the flow exhibits laminar, chaotic, or turbulent behavior [1, 2, 3, 4, 5]. This property underpins much of the modern mathematical theory of fluid dynamics and plays a central role in the analysis of long-time behavior, including the existence of absorbing sets, global attractors, and invariant measures.

Accurate numerical approximation of the NSE over long time intervals is essential in many applications, particularly when one is interested in the *climate* of the model, such as long-time statistical quantities, time-averaged observables, or asymptotic regimes, rather than short-time transient dynamics. For such purposes, it is highly desirable that numerical schemes inherit the uniform-in-time boundedness of the continuous system, that is, they are *long-time structure preserving*. Numerical methods that fail to maintain this fundamental stability property may exhibit artificial energy growth, spurious numerical instabilities, or incorrect long-time statistics, even if they are formally consistent and stable over finite time intervals.

Beyond long-time stability, higher-order time integration schemes are also highly desirable, as they allow relatively large time steps while maintaining a prescribed error tolerance. Moreover, variable time-stepping strategies are essential for enhancing computational efficiency, enabling the use of larger time steps during slow temporal evolution and smaller steps when rapid dynamics are present.

The goal of this work is to develop and analyze numerical algorithms for the incompressible Navier–Stokes equations that enjoy the following three properties: (i) uniform-in-time bounds on the solution for all positive time under variable stepping; (ii) second-order accuracy in time under variable step sizes; (iii) embedded adaptive time-stepping that combines long-time stability and automatic time-step control.

**Long-time stability and numerical discretizations.** Early numerical investigations of long-time stability for the NSE focused primarily on fully implicit schemes. Under additional assumptions on the continuous solution, long-time stability results were es-

tablished for classical methods such as the backward Euler and Crank–Nicolson schemes [6, 7, 8, 9]. To reduce computational cost while retaining stability, significant effort has been devoted to linearly implicit and semi-implicit methods. Representative results include unconditional stability and dissipativity analyses for semi-implicit Euler and projection-type schemes [10, 11, 12], as well as unconditional long-time stability results for higher-order schemes such as BDF2 [13]. Further developments can be found in [14, 15, 16, 17]. Despite their favorable stability properties, these approaches typically require solving non-symmetric linear systems with variable coefficients at each time step, which can be computationally expensive.

To improve efficiency, it is natural to treat the nonlinear advection term explicitly while discretizing the viscous term implicitly. This strategy allows reuse of the same linear operator at each time step. For the two-dimensional NSE in vorticity form, long-time stability and statistical convergence results were established for first- and second-order IMEX schemes in [18, 19], with higher-order extensions in [20]. However, the stability of these IMEX schemes typically relies on time-step restrictions depending on the Reynolds number, which can severely limit their effectiveness.

**Exponential time differencing and SAV methodologies.** Exponential time differencing (ETD) methods provide an appealing alternative for stiff nonlinear systems by treating the linear part exactly and incorporating the nonlinear term via Duhamel’s principle. ETD schemes offer high-order temporal accuracy and strong stability properties and can be efficiently implemented using FFT-based techniques in periodic domains. They have been applied to a wide class of semilinear parabolic equations [21, 22, 23, 24, 25] as well as some nonlinear equations with mild nonlinearities [26, 27, 28, 29]. The last paper addresses the variable-step case. See also [30] for ETD-Adams–Bashforth–Moulton type schemes. Nevertheless, the application of ETD methods to the incompressible NSE is nontrivial. While several ETD-based approaches have been proposed [31, 30, 32, 33, 34], rigorous results on their long-time stability remain unavailable.

In parallel, the scalar auxiliary variable (SAV) methodology and its variants have emerged as powerful tools for constructing energy-stable schemes [35, 36, 37, 38, 39]. A different extension, sometimes dubbed the ZEC method, utilizes the energy conservation property of the nonlinear term and has achieved notable success for the NSE and related

systems [40, 41, 42, 43, 44, 45, 46]. However, most existing SAV-based approaches focus on finite-time stability or impose restrictive assumptions. In the absence of external forcing, solutions decay to zero as time tends to infinity, rendering the long-time dynamics trivial.

Recently, one of the authors and collaborators developed a second-order mean-reverting SAV method (BDF2-mr-SAV) that guarantees uniform-in-time bounds under nontrivial forcing [47, 48]. This scheme is highly efficient, requiring only two Stokes solves per time step. However, a long-time stable variable-step extension remains elusive. To the best of our knowledge, no higher-order variable-step schemes preserve uniform-in-time energy bounds under general forcing.

**Contributions of this work.** We develop efficient high-order time-stepping schemes for the incompressible NSE by integrating mean-reverting SAV formulations [48, 47], dynamic second-order SAV corrections [49], and exponential time-differencing multistep methods. The proposed schemes are fully linear in the fluid variables, and the auxiliary variable is updated using only past information.

The main contributions are summarized as follows:

- An unconditionally stable variable-step second-order ETD-mr-SAV scheme under periodic boundary conditions.
- Rigorous unconditional uniform-in-time  $L^\infty(0, \infty; L^2)$  bounds under variable step sizes without time-step restriction.
- Explicit treatment of nonlinear advection while preserving long-time stability.
- An embedded adaptive scheme combining long-time stability and automatic error control.

To the best of our knowledge, this is the first theoretical study of higher-order variable-step methods for the NSE that rigorously preserve uniform-in-time energy bounds under external forcing.

The remainder of the paper is organized as follows. Section 2 introduces the reformulation and functional setting. Section 3 presents the numerical algorithm. Section 4 establishes unconditional long-time stability. Numerical experiments are reported in Section 5. Concluding remarks are given in Section 6.

## 2. Preliminaries and the extended system with mean-reverting SAV reformulation

In this section, we introduce the function spaces and an extended system for the incompressible Navier–Stokes equations, which form the foundation for our construction of efficient and unconditionally long-time stable numerical schemes.

### 2.1. Function spaces

Throughout this paper, we denote by  $\langle \cdot, \cdot \rangle$  the duality pairing between  $\dot{H}_{\text{per}}^1$  and  $H_{\text{per}}^{-1}$  induced by the  $L^2$  inner product, and by  $\|\cdot\|$  the norm in  $L^2(\Omega)$ . We recall the mean-zero periodic Sobolev space

$$(\dot{H}_{\text{per}}^k(\Omega))^d = \text{the closure of } d\text{-dimensional zero-mean trigonometric polynomials in } (H^k(\Omega))^d, \quad (2.1)$$

and its divergence-free subspaces for  $k = 0, 1$ ,

$$\begin{aligned} \mathbf{H} &= \left\{ \mathbf{u} \in (\dot{H}_{\text{per}}^0(\Omega))^d : \nabla \cdot \mathbf{u} = 0 \right\}, \\ \mathbf{V} &= \left\{ \mathbf{u} \in (\dot{H}_{\text{per}}^1(\Omega))^d : \nabla \cdot \mathbf{u} = 0 \right\}. \end{aligned} \quad (2.2)$$

These spaces are endowed with the corresponding  $(H^k(\Omega))^d$  norms, denoted by  $\|\cdot\|_k$ .

Let  $\mathcal{P} : (\dot{L}^2(\Omega))^d \rightarrow \mathbf{H}$  be the Leray–Hopf orthogonal projection operator from  $(\dot{L}^2(\Omega))^d$  onto  $\mathbf{H}$ . We can recast the NSE (1.1) as

$$\frac{\partial \mathbf{u}}{\partial t} + \nu \mathcal{L} \mathbf{u} + B(\mathbf{u}, \mathbf{u}) = \mathbf{F}, \quad (2.3)$$

where  $\mathcal{L} \mathbf{u} = -\mathcal{P} \Delta \mathbf{u}$  is the Stokes operator,  $B(\mathbf{u}, \mathbf{v}) = \mathcal{P}(\mathbf{u} \cdot \nabla \mathbf{v})$ , and  $\mathbf{F} = \mathcal{P}(\mathbf{f})$ . We point out that the Leray–Hopf projection can be calculated explicitly and efficiently in Fourier space. The following property of the nonlinear term is central to the construction of our scheme:

$$\langle B(\mathbf{u}, \mathbf{v}), \mathbf{v} \rangle = 0, \quad \forall \mathbf{u}, \mathbf{v} \in \mathbf{V}.$$

For notational simplicity, we often use  $\mathbf{u}(t)$  or  $\mathbf{u}$  to denote  $\mathbf{u}(\mathbf{x}, t) : \Omega \times \mathbb{R}^+ \mapsto \mathbb{R}^d$ , where  $\mathbb{R}^+ = [0, \infty)$ . A similar convention is applied to other vector- and scalar-valued functions. Additionally, boldface letters are used to represent vectors and vector spaces.

In the two-dimensional case, the NSE can be equivalently reformulated into the vorticity–streamfunction formulation as presented in (1.2). In this formulation, the non-linear term  $B(\mathbf{u}, \omega) = \mathbf{u} \cdot \nabla \omega$  also satisfies the conservation property

$$\langle B(\mathbf{v}, \omega), \omega \rangle = 0, \quad \forall \omega \in V, \mathbf{v} \in \mathbf{V}.$$

The corresponding Sobolev spaces are  $H = \dot{H}_{\text{per}}^0(\Omega)$  and  $V = \dot{H}_{\text{per}}^1(\Omega)$ .

For (1.2), both the algorithm design and theoretical analysis follow an identical logic to those developed for the primitive variable formulation. For brevity, we focus on the primitive variable formulation in the sequel.

## 2.2. Extended system with mean-reverting dynamic second-order SAV correction

To facilitate the development of efficient algorithms for the NSE (1.1) while achieving second-order accuracy and preserving long-time stability, we introduce the following extended system, which incorporates a dynamic scalar auxiliary variable  $r(t)$  and a mean-reverting term  $\gamma r$ :

$$\frac{\partial \mathbf{u}}{\partial t} + \nu \mathcal{L} \mathbf{u} + (1 - r^k) B(\mathbf{u}, \mathbf{u}) = \mathbf{F}, \quad (2.4a)$$

$$\frac{dr}{dt} + \gamma r = -(r - 1)^{k-1} \langle B(\mathbf{u}, \mathbf{u}), \mathbf{u} \rangle. \quad (2.4b)$$

Here,  $k = 2^1$ , and  $\gamma > 0$  is a user-specified mean-reverting parameter.

It is straightforward to verify that

$$|r(t)| \leq |r_0| e^{-\gamma t} + \frac{1}{\gamma} (1 - e^{-\gamma t}) \|(1 - r)^{k-1}\|_{L^\infty(0,t)} \|\langle B(\mathbf{u}, \mathbf{u}), \mathbf{u} \rangle\|_{L^\infty(0,t)}.$$

When the nonlinear term is energy conservative, that is,  $\langle B(\mathbf{u}, \mathbf{u}), \mathbf{u} \rangle \equiv 0$ , we deduce that

$$r(t) = r_0 e^{-\gamma t} \longrightarrow 0, \quad \text{as } t \rightarrow \infty.$$

Furthermore, if  $r(0) = 0$ , then  $r(t) \equiv 0$  for all  $t \geq 0$ , and we recover the original model (2.3).

Even if the initial data do not vanish, or the trilinear term is not identically zero, as may occur in numerical approximations, the mean-reverting term  $\gamma r$  will drive  $r(t)$  back

---

<sup>1</sup>We obtain a first-order scheme when  $k = 1$ .

to its desirable value 0. This motivates the terminology *mean-reverting scalar auxiliary variable* (mr-SAV).

Moreover, if  $r$  contains an error of size  $\tau$ , the induced error in the  $\mathbf{u}$  equation is of second order when  $k = 2$ . This property is particularly useful when  $r$  is approximated with only first-order accuracy. This dynamic second-order SAV correction was utilized in the gradient flow context in [49]. Related higher-order correction ideas also appeared in [50].

The introduction of  $r(t)$  facilitates the explicit treatment of the nonlinear term, while the damping term enhances stability. For  $\gamma > 0$  and  $k = 1$ , the long-time stability of discretizations of (2.4) via BDF2 and Gear's extrapolation was established in [47, 48]. If  $\gamma = 0$  and  $k = 1$ , the system reduces to the standard SAV-ZEC formulation. This approach has been extensively studied and applied to various fluid models [51, 52, 45, 53]. However, in this case, the error introduced by explicit treatment of nonlinear advection may accumulate over long-time simulations, and  $r(t)$  may deviate significantly from 0, even when  $r(0) = 0$ . Consequently, simulation results may become unreliable at large times. The introduction of  $\gamma$  renders (2.4b) dissipative and alleviates this difficulty.

### 3. Exponential time difference mr-SAV schemes

Building upon the mr-SAV extended systems presented in (2.4), we proceed to develop a second-order exponential time differencing (ETD) time-stepping scheme. We also introduce an embedded adaptive time-stepping version of our scheme by leveraging an embedded first-order scheme.

Given an arbitrary terminal time  $T$  and a set of non-overlapping time nodes  $0 = t_0 < t_1 < \dots < t_N = T$  with the  $k$ th time step size  $\tau_k = t_k - t_{k-1}$ , we allow the time partition to be non-uniform. Let  $\Psi^n$  denote the numerical approximation of  $\Psi(t)$  at time  $t_n$ , and abbreviate  $\Psi(t_n + \frac{1}{2}\tau_{n+1})$  as  $\Psi^{n+\frac{1}{2}}$ . We further introduce the extrapolation formula for  $\Psi^{n+\frac{1}{2}}$ , given by

$$\tilde{\Psi}^{n+\frac{1}{2}} = \frac{\tau_{n+1} + 2\tau_n}{2\tau_n} \Psi^n - \frac{\tau_{n+1}}{2\tau_n} \Psi^{n-1}. \quad (3.1)$$

#### 3.1. Second-order ETD mr-SAV multistep scheme

To obtain a second-order accurate approximation  $\mathbf{u}^{n+1}$ , we approximate the nonlinear terms in (2.4) using a second-order midpoint extrapolation and set  $k = 2$ . The resulting

scheme, inspired by [49], takes the form

$$\begin{cases} \frac{\partial \mathbf{u}(t)}{\partial t} + \nu \mathcal{L} \mathbf{u}(t) + (1 - (r^{n+1})^2) B(\tilde{\mathbf{u}}^{n+\frac{1}{2}}, \tilde{\mathbf{u}}^{n+\frac{1}{2}}) = \mathbf{F}^{n+\frac{1}{2}}, \\ \frac{dr(t)}{dt} + \gamma r(t) = (1 - r^{n+1}) (\varphi_1(\tau_{n+1} \gamma))^{-1} \left\langle \varphi_1(\tau_{n+1} \nu \mathcal{L}) B(\tilde{\mathbf{u}}^{n+\frac{1}{2}}, \tilde{\mathbf{u}}^{n+\frac{1}{2}}), \mathbf{u}^{n+1} \right\rangle, \end{cases} \quad (3.2)$$

for  $t \in (t_n, t_{n+1}]$ . Subsequently, by applying the variation-of-constants formula, the solution  $(\mathbf{u}^{n+1}, r^{n+1})$  to (3.2) can be expressed as

$$\begin{aligned} \mathbf{u}^{n+1} &= \varphi_0(\tau_{n+1} \nu \mathcal{L}) \mathbf{u}^n - \tau_{n+1} (1 - (r^{n+1})^2) \varphi_1(\tau_{n+1} \nu \mathcal{L}) B(\tilde{\mathbf{u}}^{n+\frac{1}{2}}, \tilde{\mathbf{u}}^{n+\frac{1}{2}}) \\ &\quad + \tau_{n+1} \varphi_1(\tau_{n+1} \nu \mathcal{L}) \mathbf{F}^{n+\frac{1}{2}}, \end{aligned} \quad (3.3a)$$

$$r^{n+1} = \varphi_0(\tau_{n+1} \gamma) r^n + \tau_{n+1} (1 - r^{n+1}) \left\langle \varphi_1(\tau_{n+1} \nu \mathcal{L}) B(\tilde{\mathbf{u}}^{n+\frac{1}{2}}, \tilde{\mathbf{u}}^{n+\frac{1}{2}}), \mathbf{u}^{n+1} \right\rangle, \quad (3.3b)$$

where  $\varphi_0(\cdot)$  and  $\varphi_1(\cdot)$  are defined by

$$\varphi_0(z) = e^{-z}, \quad \varphi_1(z) = \frac{1 - e^{-z}}{z}. \quad (3.4)$$

Following the classical SAV technique, the above second-order exponential time-differencing mean-reverting SAV two-step (ETD-mr-SAV-MS2o) scheme can be solved efficiently. The procedure is as follows:

1. Calculate the intermediate variables (via two Stokes solves):

$$\begin{aligned} \mathbf{u}_1^{n+1} &= \varphi_0(\tau_{n+1} \nu \mathcal{L}) \mathbf{u}^n + \tau_{n+1} \varphi_1(\tau_{n+1} \nu \mathcal{L}) \mathbf{F}^{n+\frac{1}{2}}, \\ \mathbf{u}_2^{n+1} &= \tau_{n+1} \varphi_1(\tau_{n+1} \nu \mathcal{L}) B(\tilde{\mathbf{u}}^{n+\frac{1}{2}}, \tilde{\mathbf{u}}^{n+\frac{1}{2}}). \end{aligned} \quad (3.5)$$

2. Compute the coefficients:

$$A^{n+1} = \langle \mathbf{u}_1^{n+1}, \mathbf{u}_2^{n+1} \rangle, \quad B^{n+1} = \|\mathbf{u}_2^{n+1}\|^2, \quad C^{n+1} = \varphi_0(\tau_{n+1} \gamma) r^n. \quad (3.6)$$

3. Determine the auxiliary variable  $r^{n+1}$  by finding the smallest root of the cubic polynomial

$$g(r) = B^{n+1} r^3 - B^{n+1} r^2 + (1 + A^{n+1} - B^{n+1}) r - (A^{n+1} - B^{n+1} + C^{n+1}). \quad (3.7)$$

4. Obtain  $\mathbf{u}^{n+1}$  from

$$\mathbf{u}^{n+1} = \mathbf{u}_1^{n+1} - (1 - (r^{n+1})^2) \mathbf{u}_2^{n+1}. \quad (3.8)$$

It is evident that the ETD-mr-SAV-MS2o scheme is computationally efficient, since only two Stokes solves (with the associated FFT) and one cubic polynomial root-finding are required per time step.

**Remark 3.1** (Solvability of the auxiliary variable). *We briefly discuss the solvability of the cubic algebraic equation (3.7). When the leading coefficient vanishes, i.e.,  $B^{n+1} = 0$ , we have  $\mathbf{u}_2^{n+1} = 0$ , which further implies  $A^{n+1} = 0$ . In this case, (3.7) reduces to a linear polynomial with leading coefficient equal to 1, and solvability is guaranteed. When  $B^{n+1} > 0$ , (3.7) is a non-degenerate cubic polynomial and hence admits at least one real root.*

*In addition, using the facts that  $\varphi_0(z) \approx 1$  and  $\varphi_1(z) \approx 1$  when  $z \ll 1$ , the skew-symmetric property of the nonlinear term  $B(\cdot, \cdot)$ , the relation  $\mathbf{u}^n - \mathbf{u}^{n-1} = \mathcal{O}(\tau_n)$ , and the assumption that the ratio of adjacent time steps satisfies  $\tau_{n+1}/\tau_n \approx 1$ , we obtain  $B^{n+1} = \mathcal{O}(\tau_{n+1}^2)$ ,  $A^{n+1} = \mathcal{O}(\tau_{n+1}^2)$ , and  $C^{n+1} = \mathcal{O}(\tau_{n+1})$ . Moreover, the first derivative of  $g(r)$  is*

$$g'(r) = 3B^{n+1}r^2 - 2B^{n+1}r + (1 + A^{n+1} - B^{n+1}),$$

*and the minimum value of  $g'(r)$  is attained at  $r = \frac{1}{3}$ , yielding  $g'(r) = 1 + A^{n+1} - \frac{4}{3}B^{n+1} > 0$  for sufficiently small time steps. This implies that  $g(r)$  is non-decreasing on  $\mathbb{R}$  and hence admits a unique root.*

*In practical computations, Newton's method is used to solve (3.7). Specifically, when  $\tau_{n+1}$  is sufficiently small,  $g'(r) > 0$  holds. In addition,  $g''(r) = 6B^{n+1}r - 2B^{n+1} = \mathcal{O}(\tau_{n+1}^2)$ . Therefore, Newton's method enjoys quadratic convergence with a favorable coefficient.*

**Remark 3.2** (Second-order accuracy). *We now give a heuristic argument for the second-order accuracy of  $\mathbf{u}$ . The numerical approximation of  $r^{n+1}$  in (3.3b) is formally first order, since  $\varphi_1(\tau_{n+1}\nu\mathcal{L}) \approx I$  when  $\tau_{n+1}$  is small, leading to the inner product term*

$$\left\langle \varphi_1(\tau_{n+1}\nu\mathcal{L})B(\tilde{\mathbf{u}}^{n+\frac{1}{2}}, \tilde{\mathbf{u}}^{n+\frac{1}{2}}), \mathbf{u}^{n+1} \right\rangle = \mathcal{O}(\tau_{n+1}).$$

*Nevertheless, (3.3a) formally achieves second-order accuracy due to the following two observations:*

1.  $(r^{n+1})^2 \tau_{n+1} \varphi_1(\tau_{n+1}\nu\mathcal{L}) B(\tilde{\mathbf{u}}^{n+\frac{1}{2}}, \tilde{\mathbf{u}}^{n+\frac{1}{2}}) = \mathcal{O}(\tau_{n+1}^3)$ .

2. The explicit Adams–Bashforth ETD multistep scheme is second order; see [30].

Indeed, note that  $\tau_{n+1}\varphi_1(\tau_{n+1}\nu\mathcal{L})B(\tilde{\mathbf{u}}^{n+\frac{1}{2}}, \tilde{\mathbf{u}}^{n+\frac{1}{2}}) = \int_0^{\tau_{n+1}} \varphi_0((\tau_{n+1}-s)\nu\mathcal{L}) B(\tilde{\mathbf{u}}^{n+\frac{1}{2}}, \tilde{\mathbf{u}}^{n+\frac{1}{2}}) ds$ , and  $B(\tilde{\mathbf{u}}^{n+\frac{1}{2}}, \tilde{\mathbf{u}}^{n+\frac{1}{2}})$  is formally a second-order approximation of  $B(\mathbf{u}(t_n + \frac{\tau_{n+1}}{2}), \mathbf{u}(t_n + \frac{\tau_{n+1}}{2}))$ . Furthermore, for two smooth functions  $g, h$  together with a second-order approximation of  $h$  at the midpoint  $h^{1/2} = h(\tau/2) + \mathcal{O}(\tau^2)$ , we have

$$\begin{aligned} \int_0^\tau g(s)(h(s) - h^{1/2}) &= \int_0^\tau g(s)(h(s) - h(\tau/2)) + \int_0^\tau g(s)(h(\tau/2) - h^{1/2}) \\ &= \int_0^\tau (g(\tau/2) + \mathcal{O}(\tau))(h'(\tau/2)(s - \tau/2) + \mathcal{O}(\tau^2)) + \int_0^\tau g(s)\mathcal{O}(\tau^2) \\ &= \mathcal{O}(\tau^3). \end{aligned}$$

Hence, the local truncation error is formally of order  $\mathcal{O}(\tau^3)$ , implying second-order accuracy in  $\mathbf{u}$  despite the first-order accuracy in  $r$ .

**Remark 3.3** (Alternative second-order schemes). There are two small variants of the ETD-mr-SAV-MS2o scheme that we briefly sketch here.

1. We may remove the operator  $(\varphi_1(\tau_{n+1}\gamma))^{-1}\varphi_1(\tau_{n+1}\nu\mathcal{L})$  from (3.2) and arrive at the following alternative scheme to (3.3a)–(3.3b):

$$\begin{aligned} \mathbf{u}^{n+1} &= \varphi_0(\tau_{n+1}\nu\mathcal{L})\mathbf{u}^n - \tau_{n+1}(1 - (r^{n+1})^2)\varphi_1(\tau_{n+1}\nu\mathcal{L})B(\tilde{\mathbf{u}}^{n+\frac{1}{2}}, \tilde{\mathbf{u}}^{n+\frac{1}{2}}) + \tau_{n+1}\varphi_1(\tau_{n+1}\nu\mathcal{L})\mathbf{F}^{n+\frac{1}{2}}, \\ r^{n+1} &= \varphi_0(\tau_{n+1}\gamma)r^n + \tau_{n+1}(1 - r^{n+1})\varphi_1(\tau_{n+1}\gamma)\langle B(\tilde{\mathbf{u}}^{n+\frac{1}{2}}, \tilde{\mathbf{u}}^{n+\frac{1}{2}}), \mathbf{u}^{n+1} \rangle. \end{aligned}$$

This alternative scheme has the same second-order accuracy for  $\mathbf{u}^{n+1}$  and the same computational complexity. Moreover, the stability analysis is similar to that of Theorem 4.3, though it may require higher regularity of the solution.

2. Another choice is to directly extrapolate the nonlinear terms, leading to the following second-order ETD mr-SAV scheme:

$$\begin{aligned} \mathbf{u}^{n+1} &= \varphi_0(\tau_{n+1}\nu\mathcal{L})\mathbf{u}^n - \tau_{n+1}(1 - (r^{n+1})^2)\varphi_1(\tau_{n+1}\nu\mathcal{L})\left(\frac{\tau_{n+1} + 2\tau_n}{2\tau_n}B(\mathbf{u}^n, \mathbf{u}^n) - \frac{\tau_{n+1}}{2\tau_n}B(\mathbf{u}^{n-1}, \mathbf{u}^{n-1})\right) + \tau_{n+1}\varphi_1(\tau_{n+1}\nu\mathcal{L})\mathbf{F}^{n+\frac{1}{2}}, \\ r^{n+1} &= \varphi_0(\tau_{n+1}\gamma)r^n + \tau_{n+1}(1 - r^{n+1})\left\langle \varphi_1(\tau_{n+1}\nu\mathcal{L})\left(\frac{\tau_{n+1} + 2\tau_n}{2\tau_n}B(\mathbf{u}^n, \mathbf{u}^n) - \frac{\tau_{n+1}}{2\tau_n}B(\mathbf{u}^{n-1}, \mathbf{u}^{n-1})\right), \mathbf{u}^{n+1} \right\rangle. \end{aligned}$$

This scheme exhibits the same stability results and similar numerical performance as (3.3a)–(3.3b). Therefore, it is only briefly introduced here and will not be analyzed further.

### 3.2. Embedded adaptive time stepping ETD mr-SAV multistep scheme

We now present an embedded adaptive time-stepping algorithm based on the long-time stable variable-step second-order scheme (3.3). This embedded adaptive scheme enables automatic error control without significant computational overhead while maintaining long-time stability.

First, we construct a first-order scheme by considering the special case of (3.3a)–(3.3b) with  $k = 1$ , which yields

$$\begin{aligned}\bar{\mathbf{u}}^{n+1} &= \varphi_0(\tau_{n+1}\nu\mathcal{L})\mathbf{u}^n - \tau_{n+1}(1 - \bar{r}^{n+1})\varphi_1(\tau_{n+1}\nu\mathcal{L})B(\tilde{\mathbf{u}}^{n+\frac{1}{2}}, \tilde{\mathbf{u}}^{n+\frac{1}{2}}) \\ &\quad + \tau_{n+1}\varphi_1(\tau_{n+1}\nu\mathcal{L})\mathbf{F}^{n+\frac{1}{2}},\end{aligned}\quad (3.9a)$$

$$\bar{r}^{n+1} = \varphi_0(\tau_{n+1}\gamma)r^n - \tau_{n+1}\left\langle \varphi_1(\tau_{n+1}\nu\mathcal{L})B(\tilde{\mathbf{u}}^{n+\frac{1}{2}}, \tilde{\mathbf{u}}^{n+\frac{1}{2}}), \bar{\mathbf{u}}^{n+1} \right\rangle,\quad (3.9b)$$

It is straightforward to verify that  $\bar{r}^{n+1}$  in (3.9a) is also of order  $\tau_{n+1}$ . Consequently,  $1 - \bar{r}^{n+1}$  provides a first-order approximation of 1, implying that  $\bar{\mathbf{u}}^{n+1}$  achieves only first-order accuracy. We therefore refer to (3.9) as the first-order exponential time-differencing mean-reverting SAV (**ETD-mr-SAV-MS1o**) scheme.

Due to its structural similarity to the ETD-mr-SAV-MS2o scheme, the intermediate values used to solve (3.3a) can be reused to compute **ETD-mr-SAV-MS1o**. Specifically, the procedure is:

1. Determine  $\bar{r}^{n+1}$  by solving the linear relation

$$\bar{r}^{n+1} = C^{n+1} + A^{n+1} + (1 - \bar{r}^{n+1})B^{n+1}. \quad (3.10)$$

2. Obtain  $\bar{\mathbf{u}}^{n+1}$  from

$$\bar{\mathbf{u}}^{n+1} = \mathbf{u}_1^{n+1} - (1 + \bar{r}^{n+1})\mathbf{u}_2^{n+1}. \quad (3.11)$$

Combining the first- and second-order ETD-mr-SAV schemes above, we construct an embedded adaptive algorithm. Following [54], the adaptive strategy is summarized in **Algorithm 1** with the time-step update function

$$A_{dp}(e_{\mathbf{u}}, e_q, \tau) = \rho \left( \min \left\{ \frac{\text{tol}_{\mathbf{u}}}{e_{\mathbf{u}}}, \frac{\text{tol}_q}{e_q} \right\} \right)^{\frac{1}{2}} \tau. \quad (3.12)$$

Here,  $\rho$  is a safety factor, and  $\text{tol}_{\mathbf{u}}$  and  $\text{tol}_q$  are prescribed tolerances for the fluid variable  $\mathbf{u}$  and the scalar auxiliary variable  $r$ , respectively. These parameters depend on the

specific problem under consideration. We refer to this adaptive time-stepping method as the **ETD-mr-SAV-MS12** scheme.

---

**Algorithm 1** ETD-mr-SAV-MS12 scheme

---

**Given:**  $\mathbf{u}^n, \mathbf{u}^{n-1}, r^n, \tau_{n+1}$ .

**Step 1.** Compute  $\mathbf{u}_1^{n+1}, \mathbf{u}_2^{n+1}$  and the coefficients  $A^{n+1}, B^{n+1}, C^{n+1}$  via (3.5) and (3.6).

**Step 2.** Compute  $r^{n+1}$  and  $\bar{r}^{n+1}$  via (3.7) and (3.10), respectively.

**Step 3.** Compute the second-order approximation  $\mathbf{u}^{n+1}$  and the first-order approximation  $\bar{\mathbf{u}}^{n+1}$  via (3.8) and (3.11), respectively.

**Step 4.** Compute  $e_{\mathbf{u}}^{n+1} = \frac{\|\bar{\mathbf{u}}^{n+1} - \mathbf{u}^{n+1}\|}{\max\{\|\bar{\mathbf{u}}^{n+1}\|, \|\mathbf{u}^{n+1}\|\}}$  and  $e_q^{n+1} = |r^{n+1} - 1|$ .

**if**  $e_{\mathbf{u}}^{n+1} \leq \text{tol}_{\mathbf{u}}$  and  $e_q^{n+1} \leq \text{tol}_q$  **then**

**Step 5.** Update  $\tau_{n+2} \leftarrow \max\{\tau_{\min}, \min\{A_{dp}(e_{\mathbf{u}}^{n+1}, e_q^{n+1}, \tau_{n+1}), \tau_{\max}\}\}$ .

**else**

**Step 6.** Reset  $\tau_{n+1} \leftarrow \max\{\tau_{\min}, \min\{A_{dp}(e_{\mathbf{u}}^{n+1}, e_q^{n+1}, \tau_{n+1}), \tau_{\max}\}\}$ .

**Step 7.** Go to **Step 1**.

**end if**

---

**Remark 3.4.** In this adaptive time-stepping setting, one may instead use a first-order single-step scheme obtained by replacing  $\tilde{\mathbf{u}}^{n+1/2}$  with  $\mathbf{u}^n$ . However, to construct an embedded adaptive algorithm without additional computational cost, we choose the first-order two-step ETD-mr-SAV scheme so that the intermediate computations can be shared with the ETD-mr-SAV-MS2o scheme.

#### 4. Long-time stability of the ETD-mr-SAV scheme

The purpose of this section is to derive uniform-in-time energy bounds for the ETD-mr-SAV scheme proposed in the previous section. More precisely, we establish  $L^\infty(0, \infty; L^2)$  stability (together with a corresponding cumulative dissipation estimate) under uniformly bounded forcing.

We first recall several elementary properties of the two functions  $\varphi_j$ ,  $j = 0, 1$ , that are related to ETD schemes.

**Lemma 4.1.** The functions  $\varphi_i$  defined in (3.4) satisfy:

(1)  $\varphi_i(z)$  is decreasing for  $i = 0, 1$ .

(2)  $z\varphi_1(z) + \varphi_0(z) = 1$ .

$$(3) \ 0 \leq \varphi_0(z) \leq 1, \ 0 \leq \varphi_1(z) \leq 1, \text{ and } 1 + \frac{z}{2} \leq (\varphi_1(z))^{-1} \leq 1 + z, \quad \forall z \geq 0.$$

$$(4) \ (\varphi_1(z))^{-1} \geq z, \quad \forall z \in \mathbb{R}^+.$$

It is then straightforward to verify, with the help of the Fourier representation, that for any  $\mathbf{h} \in \mathbf{V}$  and  $\tau > 0$ ,

$$\begin{aligned} \varphi_1(\tau\nu\mathcal{L})\mathbf{h} &= (\tau\nu\mathcal{L})^{-1}(I - e^{-\tau\nu\mathcal{L}})\mathbf{h} = \sum_{\mathbf{k} \in \mathbb{Z}^d \setminus \{0\}} \frac{1 - e^{-\tau\nu\lambda_{\mathbf{k}}}}{\tau\nu\lambda_{\mathbf{k}}} \hat{\mathbf{h}}_{\mathbf{k}} e^{i\mathbf{k} \cdot \mathbf{x}}, \\ (\varphi_1(\tau\nu\mathcal{L}))^{-1}\mathbf{h} &= (I - e^{-\tau\nu\mathcal{L}})^{-1}(\tau\nu\mathcal{L})\mathbf{h} = \sum_{\mathbf{k} \in \mathbb{Z}^d \setminus \{0\}} \frac{\tau\nu\lambda_{\mathbf{k}}}{1 - e^{-\tau\nu\lambda_{\mathbf{k}}}} \hat{\mathbf{h}}_{\mathbf{k}} e^{i\mathbf{k} \cdot \mathbf{x}}, \end{aligned} \quad (4.1)$$

where  $\lambda_{\mathbf{k}}$  denotes the eigenvalue of the Stokes operator  $\mathcal{L}$  associated with the divergence-free Fourier mode  $\hat{\mathbf{h}}_{\mathbf{k}} e^{i\mathbf{k} \cdot \mathbf{x}}$ , with  $\mathbf{k} \cdot \hat{\mathbf{h}}_{\mathbf{k}} = 0$ .

We also recall the Poincaré inequality

$$\|\mathbf{h}\| \leq \frac{1}{\sqrt{\lambda_1}} \|\mathcal{L}^{1/2}\mathbf{h}\|, \quad \forall \mathbf{h} \in \mathbf{V}, \quad (4.2)$$

where  $\lambda_1 > 0$  is the smallest eigenvalue of  $\mathcal{L}$ .

Combining the spectral representation (4.1) with Lemma 4.1, we obtain the following simple estimates.

**Lemma 4.2.** *For any  $\mathbf{h} \in \mathbf{V}$  and  $\tau > 0$ , the following estimates hold:*

$$\|\mathbf{h}\|^2 = \tau\nu \|(\varphi_1(\tau\nu\mathcal{L}))^{1/2}\mathcal{L}^{1/2}\mathbf{h}\|^2 + \|(\varphi_0(\tau\nu\mathcal{L}))^{1/2}\mathbf{h}\|^2, \quad (4.3)$$

$$\|(\varphi_1(\tau\nu\mathcal{L}))^{1/2}\mathbf{h}\|^2 \leq \|\mathbf{h}\|^2, \quad (4.4)$$

$$\|\mathbf{h}\|^2 + \frac{\tau\nu}{2} \|\mathcal{L}^{1/2}\mathbf{h}\|^2 \leq \|(\varphi_1(\tau\nu\mathcal{L}))^{-1/2}\mathbf{h}\|^2 \leq \|\mathbf{h}\|^2 + \tau\nu \|\mathcal{L}^{1/2}\mathbf{h}\|^2, \quad (4.5)$$

and

$$\|(\varphi_1(\tau\nu\mathcal{L}))^{-1/2}\mathbf{h}\|^2 \geq \tau\nu \|\mathcal{L}^{1/2}\mathbf{h}\|^2. \quad (4.6)$$

#### 4.1. Long-time stability for the ETD-mr-**SAV-MS2o** scheme

We derive an  $L^\infty(0, \infty; L^2)$  bound for the **ETD-mr-**SAV-MS2o**** scheme (3.3). The same argument is also applicable to the **ETD-mr-**SAV-MS1o**** scheme. Throughout the proof we use Lemmas 4.1–4.2 and the Poincaré inequality.

**Theorem 4.3.** Assume  $(\mathbf{u}^i, r^i) \in ((\dot{H}_{per}^\alpha(\Omega))^d \cap \mathbf{H}) \times \mathbb{R}$  for  $i = 0, 1$  with  $\alpha \geq \frac{3}{4}$ , and  $\mathbf{F} \in L^\infty(0, \infty; \mathbf{H})$ . Let

$$\theta := \min\{\nu\lambda_1, \gamma\} > 0. \quad (4.7)$$

Then for all  $n \geq 1$ , the ETD-mr-SAV-MS2o scheme is long-time stable in the sense that

$$\|\mathbf{u}^{n+1}\|^2 + |r^{n+1} + 1|^2 \leq e^{-\theta \sum_{i=1}^n \tau_{i+1}} (\|\mathbf{u}^1\|^2 + |r^1 + 1|^2) + \frac{1}{\theta} \left( \frac{1}{\nu\lambda_1} \|\mathbf{F}\|_{L^\infty(0, \infty; \mathbf{H})}^2 + \gamma \right). \quad (4.8)$$

*Proof.* We rewrite the scheme in a form suitable for energy estimates. Using

$$e^{-\tau_{n+1}\nu\mathcal{L}} - I = -\tau_{n+1}\nu\mathcal{L}\varphi_1(\tau_{n+1}\nu\mathcal{L}), \quad e^{-\tau_{n+1}\gamma} - 1 = -\tau_{n+1}\gamma\varphi_1(\tau_{n+1}\gamma),$$

the ETD-mr-SAV-MS2o scheme (3.3) can be rewritten as

$$\begin{aligned} & \mathbf{u}^{n+1} - \mathbf{u}^n + \tau_{n+1}\nu\mathcal{L}\varphi_1(\tau_{n+1}\nu\mathcal{L})\mathbf{u}^n \\ &= \tau_{n+1}\varphi_1(\tau_{n+1}\nu\mathcal{L}) \left( \mathbf{F}^{n+\frac{1}{2}} - (1 - (r^{n+1})^2)B(\tilde{\mathbf{u}}^{n+\frac{1}{2}}, \tilde{\mathbf{u}}^{n+\frac{1}{2}}) \right), \end{aligned} \quad (4.9)$$

and

$$\begin{aligned} & r^{n+1} - r^n + \tau_{n+1}\gamma\varphi_1(\tau_{n+1}\gamma)(r^n + 1) \\ &= \tau_{n+1}(1 - r^{n+1}) \left\langle \varphi_1(\tau_{n+1}\nu\mathcal{L})B(\tilde{\mathbf{u}}^{n+\frac{1}{2}}, \tilde{\mathbf{u}}^{n+\frac{1}{2}}), \mathbf{u}^{n+1} \right\rangle + \tau_{n+1}\gamma\varphi_1(\tau_{n+1}\gamma). \end{aligned} \quad (4.10)$$

Consider  $((4.9), 2\mathbf{u}^{n+1}) + ((4.10), 2(r^{n+1} + 1))$ . Note that the nonlinear term involving  $B(\cdot, \cdot)$  cancels since

$$-(1 - (r^{n+1})^2) + (1 - r^{n+1})(r^{n+1} + 1) = 0.$$

Using the identities  $2(a - b, a) = \|a\|^2 - \|b\|^2 + \|a - b\|^2$  and  $(a, b) = \|a\|^2 + \|b\|^2 - \|a - b\|^2$ , we obtain

$$\begin{aligned} & \|\mathbf{u}^{n+1}\|^2 - \|\mathbf{u}^n\|^2 + \|\mathbf{u}^{n+1} - \mathbf{u}^n\|^2 + \|(\tau_{n+1}\nu\mathcal{L}\varphi_1(\tau_{n+1}\nu\mathcal{L}))^{1/2}\mathbf{u}^{n+1}\|^2 \\ &+ \|(\tau_{n+1}\nu\mathcal{L}\varphi_1(\tau_{n+1}\nu\mathcal{L}))^{1/2}\mathbf{u}^n\|^2 - \|(\tau_{n+1}\nu\mathcal{L}\varphi_1(\tau_{n+1}\nu\mathcal{L}))^{1/2}(\mathbf{u}^{n+1} - \mathbf{u}^n)\|^2 \\ &+ |r^{n+1} + 1|^2 - |r^n + 1|^2 + |r^{n+1} - r^n|^2 + \tau_{n+1}\gamma\varphi_1(\tau_{n+1}\gamma)|r^{n+1} + 1|^2 \\ &+ \tau_{n+1}\gamma\varphi_1(\tau_{n+1}\gamma)|r^n + 1|^2 - \tau_{n+1}\gamma\varphi_1(\tau_{n+1}\gamma)|r^{n+1} - r^n|^2 \\ &= \left\langle \frac{\mathcal{L}^{-1}}{\nu} \tau_{n+1}\nu\mathcal{L}\varphi_1(\tau_{n+1}\nu\mathcal{L}) \mathbf{F}^{n+\frac{1}{2}}, 2\mathbf{u}^{n+1} \right\rangle + \left\langle 2\tau_{n+1}\gamma\varphi_1(\tau_{n+1}\gamma), r^{n+1} + 1 \right\rangle. \end{aligned} \quad (4.11)$$

We now estimate the right-hand side. For the first term, by the Cauchy–Schwarz and Young inequalities,

$$\begin{aligned} & \left\langle \frac{\mathcal{L}^{-1}}{\nu} \tau_{n+1} \nu \mathcal{L} \varphi_1(\tau_{n+1} \nu \mathcal{L}) \mathbf{F}^{n+\frac{1}{2}}, 2\mathbf{u}^{n+1} \right\rangle \\ & \leq \|(\tau_{n+1} \nu \mathcal{L} \varphi_1(\tau_{n+1} \nu \mathcal{L}))^{1/2} \mathbf{u}^{n+1}\|^2 + \frac{1}{\nu^2} \|(\tau_{n+1} \nu \mathcal{L} \varphi_1(\tau_{n+1} \nu \mathcal{L}))^{1/2} \mathcal{L}^{-1} \mathbf{F}^{n+\frac{1}{2}}\|^2 \quad (4.12) \\ & \leq \|(\tau_{n+1} \nu \mathcal{L} \varphi_1(\tau_{n+1} \nu \mathcal{L}))^{1/2} \mathbf{u}^{n+1}\|^2 + \frac{\tau_{n+1}}{\nu \lambda_1} \|\mathbf{F}^{n+\frac{1}{2}}\|^2. \end{aligned}$$

For the second term, similarly,

$$\begin{aligned} \langle 2\tau_{n+1} \gamma \varphi_1(\tau_{n+1} \gamma), r^{n+1} + 1 \rangle & \leq \tau_{n+1} \gamma \varphi_1(\tau_{n+1} \gamma) |r^{n+1} + 1|^2 + \tau_{n+1} \gamma \varphi_1(\tau_{n+1} \gamma) \\ & \leq \tau_{n+1} \gamma \varphi_1(\tau_{n+1} \gamma) |r^{n+1} + 1|^2 + \tau_{n+1} \gamma. \end{aligned} \quad (4.13)$$

Substituting (4.12) and (4.13) into (4.11) cancels the terms  $\|(\tau_{n+1} \nu \mathcal{L} \varphi_1(\tau_{n+1} \nu \mathcal{L}))^{1/2} \mathbf{u}^{n+1}\|^2$  and  $\tau_{n+1} \gamma \varphi_1(\tau_{n+1} \gamma) |r^{n+1} + 1|^2$  on both sides. By Lemma 4.1, the following differences are non-negative:

$$\begin{aligned} \|\mathbf{u}^{n+1} - \mathbf{u}^n\|^2 - \|(\tau_{n+1} \nu \mathcal{L} \varphi_1(\tau_{n+1} \nu \mathcal{L}))^{1/2} (\mathbf{u}^{n+1} - \mathbf{u}^n)\|^2 & \geq 0, \\ |r^{n+1} - r^n|^2 - \tau_{n+1} \gamma \varphi_1(\tau_{n+1} \gamma) |r^{n+1} - r^n|^2 & \geq 0. \end{aligned}$$

Consequently, (4.11) reduces to

$$\begin{aligned} \|\mathbf{u}^{n+1}\|^2 + |r^{n+1} + 1|^2 & \leq \|\mathbf{u}^n\|^2 + |r^n + 1|^2 - \tau_{n+1} \nu \left\| (\mathcal{L} \varphi_1(\tau_{n+1} \nu \mathcal{L}))^{\frac{1}{2}} \mathbf{u}^n \right\|^2 \quad (4.14) \\ & \quad - \tau_{n+1} \gamma \varphi_1(\tau_{n+1} \gamma) |r^n + 1|^2 + \tau_{n+1} \left( \frac{1}{\nu \lambda_1} \|\mathbf{F}^{n+\frac{1}{2}}\|^2 + \gamma \right). \end{aligned}$$

In order to derive the desired estimate that includes an exponential decay estimate of the impact of the initial data, we utilize Lemma 4.2, cf. (4.3) with  $\varphi_0(z) = e^{-z}$ , and we have

$$\begin{aligned} & \|\mathbf{u}^n\|^2 - \tau_{n+1} \nu \left\| (\mathcal{L} \varphi_1(\tau_{n+1} \nu \mathcal{L}))^{\frac{1}{2}} \mathbf{u}^n \right\|^2 \\ & = \|(\varphi_0(\tau_{n+1} \nu \mathcal{L}))^{\frac{1}{2}} \mathbf{u}^n\|^2 = \|e^{-\tau_{n+1} \nu \mathcal{L}/2} \mathbf{u}^n\|^2 \leq e^{-\tau_{n+1} \nu \lambda_1} \|\mathbf{u}^n\|^2. \end{aligned} \quad (4.15)$$

Likewise,

$$|r^n + 1|^2 - \tau_{n+1} \gamma \varphi_1(\tau_{n+1} \gamma) |r^n + 1|^2 = \varphi_0(\tau_{n+1} \gamma) |r^n + 1|^2 = e^{-\tau_{n+1} \gamma} |r^n + 1|^2. \quad (4.16)$$

Combining (4.14)–(4.16) and setting  $\theta = \min\{\nu \lambda_1, \gamma\}$  yields the one-step inequality

$$\|\mathbf{u}^{n+1}\|^2 + |r^{n+1} + 1|^2 \leq e^{-\theta \tau_{n+1}} (\|\mathbf{u}^n\|^2 + |r^n + 1|^2) + \tau_{n+1} \left( \frac{1}{\nu \lambda_1} \|\mathbf{F}^{n+\frac{1}{2}}\|^2 + \gamma \right). \quad (4.17)$$

Iterating (4.17) and using  $\|\mathbf{F}^{k+\frac{1}{2}}\| \leq \|\mathbf{F}\|_{L^\infty(0,\infty;\mathbf{H})}$ , we obtain

$$\begin{aligned} \|\mathbf{u}^{n+1}\|^2 + |r^{n+1} + 1|^2 &\leq e^{-\theta \sum_{i=1}^n \tau_{i+1}} (\|\mathbf{u}^1\|^2 + |r^1 + 1|^2) \\ &\quad + \sum_{i=1}^n e^{-\theta \sum_{j=i+1}^n \tau_{j+1}} \tau_{i+1} \left( \frac{1}{\nu \lambda_1} \|\mathbf{F}\|_{L^\infty(0,\infty;\mathbf{H})}^2 + \gamma \right). \end{aligned} \quad (4.18)$$

Denote  $S_i^n = \sum_{j=i}^n \tau_{j+1}$ . Then  $0 = S_{n+1}^n < S_n^n = \tau_{n+1} < \dots < S_1^n = \sum_{j=1}^n \tau_{j+1}$ , so  $\{S_j^n\}_{j=1}^n$  forms a partition of  $[0, S_1^n]$ . Moreover,  $\tau_{j+1} = S_j^n - S_{j+1}^n$  and  $e^{-\theta s}$  is decreasing in  $s$ . Hence,

$$\sum_{i=1}^n e^{-\theta \sum_{j=i+1}^n \tau_{j+1}} \tau_{i+1} = \sum_{i=1}^n e^{-\theta S_{i+1}^n} (S_i^n - S_{i+1}^n) \leq \int_0^{S_1^n} e^{-\theta x} dx = \frac{1 - e^{-\theta S_1^n}}{\theta}, \quad (4.19)$$

where we used the fact that the right-end Riemann sum of a monotonically decreasing function is bounded by the corresponding integral. Consequently, we obtain (4.8), which completes the proof.  $\square$

**Remark 4.1.** *As in the ETD-mr-SAV-MS2o case, the stability estimate only requires  $\mathbf{u}^0, \mathbf{u}^1 \in \mathbf{H}$ . The assumption  $\alpha \geq \frac{3}{4}$  is used to ensure that  $B(\tilde{\mathbf{u}}^{n+\frac{1}{2}}, \tilde{\mathbf{u}}^{n+\frac{1}{2}}) \in \mathbf{V}'$  and  $\mathbf{u}^{n+1} \in (\dot{H}_{per}^\alpha)^d \cap \mathbf{H}$ , so that the scheme is well-defined.*

## 5. Numerical experiments

In this section, we report several numerical experiments that illustrate the temporal accuracy, long-time stability, and practical performance of the proposed schemes, including the adaptive scheme and its automatic error control capability. In particular, we verify the expected temporal convergence order under variable time stepping (in the spirit of [55]), demonstrate the ability of the adaptive strategy to adjust time-step sizes according to the speed of temporal evolution while maintaining prescribed error tolerances, and test long-time stability in a Kolmogorov forcing setting. For the Kolmogorov flow, we further provide a comparative study in terms of long-time boundedness and statistical consistency of representative quantities.

All simulations are performed for the two-dimensional NSE in a periodic box. A Fourier spectral method is used for spatial discretization. Since solutions to the NSE are analytic in space for positive time under spatially analytic forcing [2], the spatial discretization error is negligible compared with the temporal discretization error due

to spectral accuracy. The Leray projector  $\mathcal{P}$  introduced in (2.3) can be implemented conveniently in Fourier space via

$$\mathcal{P}\mathbf{u} = \mathbf{u} - \nabla(\Delta^{-1}\nabla \cdot \mathbf{u}).$$

Moreover, for the two-dimensional examples considered below (Examples 5.1–5.2), we employ the vorticity–streamfunction formulation (1.2), in which the pressure term is eliminated and incompressibility is automatically satisfied.

### 5.1. Convergence test

**Example 5.1.** *[Accuracy test] In this example,  $\Omega = (0, 2\pi)^2$ ,  $\nu = 10^{-4}$ , and the final time is  $T = 1$ . The initial condition is specified as*

$$u = 0.2 \sin(4y) \cos(2x), \quad v = -0.1 \sin(2x) \cos(4y),$$

and the external force is given by

$$\mathbf{f}(x, y) = \begin{pmatrix} 0 \\ \sin(x) \end{pmatrix}.$$

For spatial discretization, 256 Fourier modes are used. To evaluate accuracy and efficiency, we take as a reference solution the result produced by the ETDRK4 scheme [56] with a uniform time step  $\tau = 0.1 \times 2^{-10} \approx 10^{-4}$ .

We set the mean-reverting parameter  $\gamma = 100$  and solve the problem using the ETD-mr-SAV-MS1o and ETD-mr-SAV-MS2o schemes. We first consider uniform time steps. Specifically, we perform simulations with  $\tau = 0.1 \times 2^{-k}$ , where  $k = 0, 1, \dots, 6$ , and compute the errors of the velocity, vorticity, and auxiliary variable at the final time  $T = 1$ . The corresponding results are reported in Figure 1.

From Figure 1, we observe that both schemes achieve the expected temporal convergence rates for the  $L^2$  errors of the velocity and vorticity. For the auxiliary variable error (measured by  $|r|$ ), the observed convergence behavior is consistent with the design of the schemes: the first- and second-order methods exhibit convergence rates matching their formal orders.

Next, we examine accuracy under variable time stepping. Following [55], we generate a variable-step sequence  $\{\tau_n\}$  by applying a 10% perturbation to the uniform step size

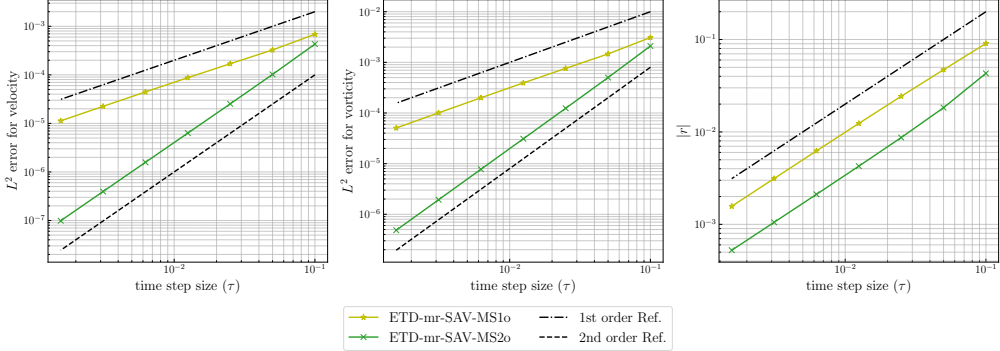


Figure 1: The  $L^2$  error of velocity (left), vorticity (middle), and absolute error of the auxiliary variable (right), computed by ETD-mr-SAV-MS1o and ETD-mr-SAV-MS2o at  $T = 1$ , plotted against the time-step size  $\tau = 0.1 \times 2^{-k}$ , for  $k = 0, 1, \dots, 6$ .

$1/N$ . Errors are again computed at the final time  $T = 1$ , and the results are presented in Figure 2. The figure indicates that the proposed schemes remain robust under variable time steps, and the observed convergence order is consistent with that obtained under uniform time stepping.

### 5.2. Long time stability

**Example 5.2.** [Long-time stability] *In this example, we simulate the Kolmogorov flow to compare the long-time performance of different schemes. We consider the two-dimensional periodic NSE on  $(0, 2\pi)^2$  in vorticity–streamfunction form (1.2), with external forcing*

$$f(x, y; t) = m \cos(my), \quad (5.1)$$

*following [57]. The corresponding steady-state solution (the basic Kolmogorov flow) is given by the streamfunction  $\psi(x, y) = -\frac{1}{\nu m^3} \cos(my)$ . The basic flow is stable for sufficiently small Reynolds number (large  $\nu$ ); when the Reynolds number exceeds a critical value, the flow loses stability and nontrivial time-dependent structures may emerge.*

We first verify long-time stability for the Kolmogorov forcing with two sets of parameters, covering both a relatively stable regime near the basic flow and a regime exhibiting bursting behavior.

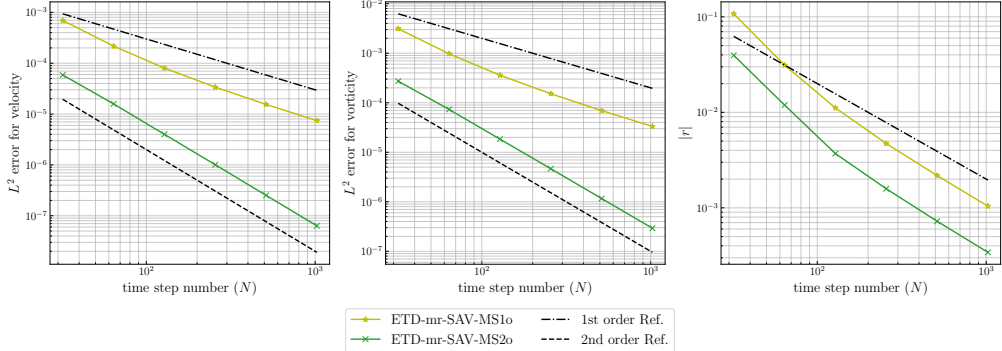


Figure 2: The  $L^2$  error of velocity (left), vorticity (middle), and absolute error of the auxiliary variable (right), computed by ETD-mr-SAV-MS1o and ETD-mr-SAV-MS2o at  $T = 1$ , plotted against the number of time steps  $N = 2^k$  under a 10% perturbed variable-step sequence, for  $k = 5, \dots, 10$ .

For the relatively stable case, we take  $m = 2$ ,  $\nu = 1/20$ , and  $\gamma = 1000$ . The initial streamfunction is a perturbation of the steady state,

$$\psi_0(x, y) = -\frac{1}{\nu m^3} \cos(my) + 0.001 \cos(mx) \cos(my). \quad (5.2)$$

We adopt two approaches up to  $T = 1000$ : (1) the ETD-mr-SAV-MS2o scheme with uniform time steps  $\tau = 0.01, 0.005, 0.0025$ ; and (2) the adaptive ETD-mr-SAV-MS12 scheme with parameters

$$\rho = 0.95, \quad \text{tol}_u = \text{tol}_q = 10^{-4}, \quad \tau_{\min} = 1 \times 10^{-5}, \quad \tau_{\max} = 1 \times 10^{-2}. \quad (5.3)$$

Figure 3 shows the evolution of the  $L^2$  norm of vorticity (enstrophy) over the entire interval. We observe that the enstrophy remains uniformly bounded for both fixed-step and adaptive simulations, consistent with the long-time stability theory established in Section 4.

For the more unstable case, we consider  $m = 4$ ,  $\nu = 1/40$ , and  $\gamma = 1000$ , with the initial streamfunction again taken as a perturbation of the steady state in the form (5.2) (with the corresponding  $m$  and  $\nu$ ). The final time is  $T = 10000$ , and spatial discretization uses 256 Fourier modes. We perform two simulations: (i) a fixed-step run with  $\tau = 5 \times 10^{-4}$  using ETD-mr-SAV-MS2o; and (ii) an adaptive run using ETD-mr-SAV-MS12 with parameters (5.3).

Figure 4 shows the time evolution of enstrophy. Although individual trajectories diverge over long times, they remain uniformly bounded for both schemes, further illustrating the long-time stability of the proposed approach. The observed separation of trajectories is consistent with sensitivity to initial conditions in this regime (e.g., positive Lyapunov exponents).

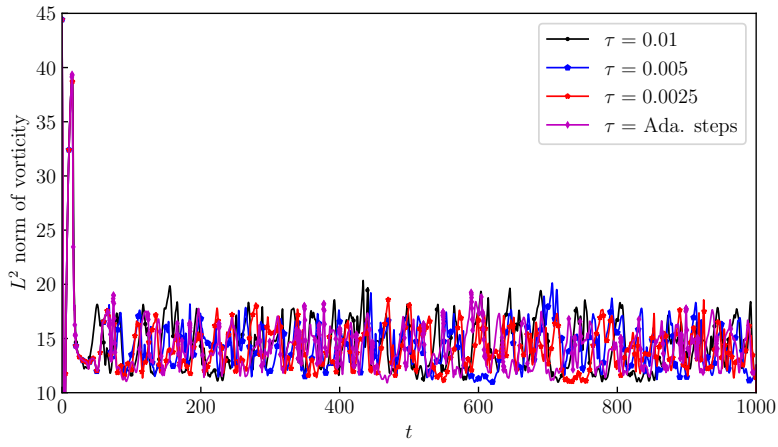


Figure 3: Evolution of the vorticity  $L^2$  norm computed by the ETD-mr-SAV-MS2o and ETD-mr-SAV-MS12 schemes for  $\nu = 1/20$  and  $m = 2$ .

### 5.3. Performance of the adaptive scheme

We now further evaluate the advantages of the adaptive time stepping scheme (ETD-mr-SAV-MS12) through both short- and long-time simulations. In the short-time setting, we emphasize automatic error control and second-order accuracy under variable step sizes; in the long-time setting, we emphasize efficiency and the ability to recover long-time statistics.

#### 5.3.1. Short-time performance: accuracy and error control

For the short-time evaluation, we adopt the parameter setting from the first Kolmogorov test with  $m = 2$  and  $\nu = 1/20$ , and choose the initial data as the flow profile at a random time between 20 and 60 from that simulation so that the trajectory starts

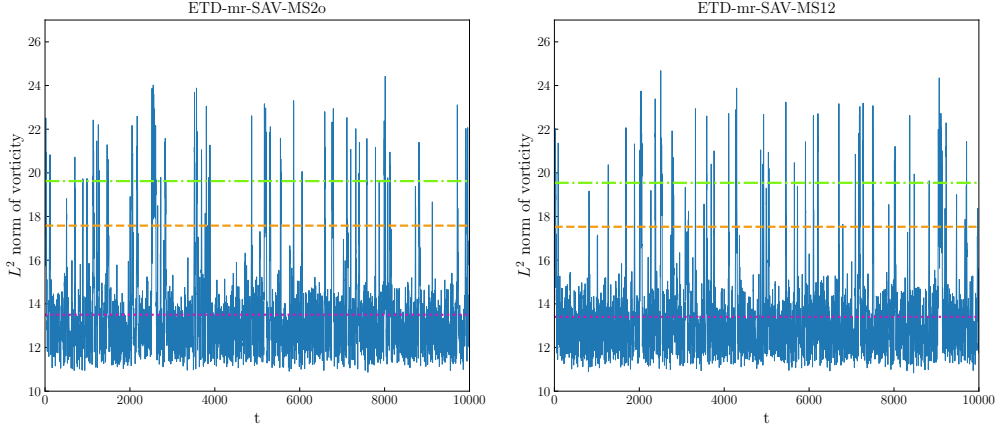


Figure 4: Enstrophy ( $L^2$  norm of vorticity) versus time computed by ETD-mr-SAV-MS2o and ETD-mr-SAV-MS12 for  $\nu = 1/40$  and  $m = 4$ . The red dotted line denotes the mean value  $\mu$ ; the orange dashed and green dash-dotted lines correspond to the thresholds  $\mu + 2\sigma$  and  $\mu + 3\sigma$ , respectively.

near the attractor. We then conduct simulations over  $t \in [0, 40]$  using (i) the ETD-mr-SAV-MS2o scheme with uniform time steps  $\tau = 0.01, 0.005, 0.0025$  and (ii) the adaptive ETD-mr-SAV-MS12 scheme.

Figure 5 reports the adaptive time-step size, the cumulative number of steps, and the corresponding error indicators used in the controller. In particular, Figures 5(a), (c), and (d) display the adaptive time step size together with the absolute value of the auxiliary variable and the relative  $L^2$  error indicator of vorticity. The results show that the adaptive algorithm adjusts the time step effectively so that the error indicators remain below the prescribed tolerance.

To assess the actual error, we employ ETDRK4 with a finer time step as a reference and report the relative  $L^2$  error in Figure 5(e). We observe that, up to  $t = 40$ , the error remains around  $10^{-4}$ , essentially matching the prescribed tolerance. Moreover, the adaptive algorithm achieves accuracy comparable to the fixed-step scheme with the finer time step ( $\tau = 0.0025$ ) while using roughly half the number of steps (Figure 5(b)). In contrast, the fixed-step method with  $\tau = 0.005$  produces substantially larger errors that exceed  $10^{-4}$ , illustrating the benefit of automatic step-size selection.

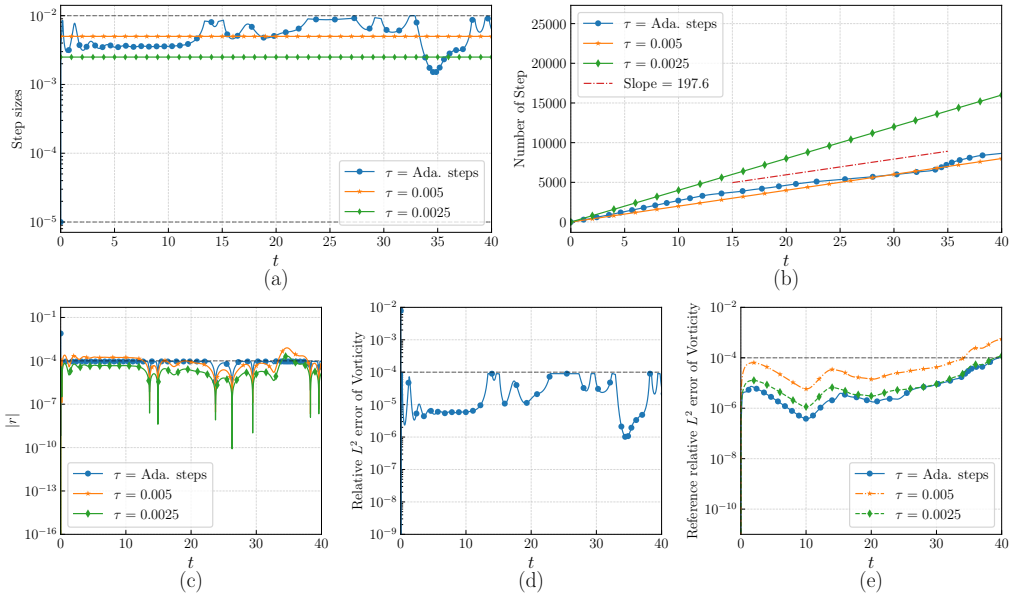


Figure 5: (a) Adaptive time step sizes as a function of time. (b) Number of steps over time for constant steps and adaptive steps. (c) Absolute value of the auxiliary variable as a function of time. (d) Relative  $L^2$  error indicator of vorticity based on numerical solutions and (e) Reference relative  $L^2$  error based on a refined ETDRK4 solution.

### 5.3.2. Long-time performance: efficiency and statistics

We further investigate the advantages of adaptive time stepping in the bursting regime with  $m = 4$  and  $\nu = 1/40$ . The results are shown in Figure 6. Figures 6(a)–(c) indicate that the adaptive scheme automatically selects smaller time steps during bursting events (spikes in enstrophy), thereby improving temporal resolution during rapid transients, while taking larger steps during relatively quiescent periods.

To quantify the relationship between time step size and enstrophy, we compute the Pearson correlation coefficient (PCC),  $PCC(x, y) = \frac{\sum(x-m_x)(y-m_y)}{\sqrt{\sum(x-m_x)^2 \sum(y-m_y)^2}}$ , where  $m_x$  and  $m_y$  denote the mean values of  $x$  and  $y$ , respectively. We obtain a PCC value of  $-0.7806$  between time step size and enstrophy, indicating a strong negative correlation: as enstrophy increases, the time step decreases. In addition, Figure 6(e) shows that the adaptive simulation requires only about one-sixth of the time steps used by the fixed-step run, demonstrating a substantial efficiency gain while preserving long-time stability.

We finally examine long-time statistical consistency. We consider the probability density function (PDF) of enstrophy and compute the total variation distance between the enstrophy distributions produced by different schemes using the same uniform temporal sampling. As shown in Figure 7, the PDFs are nearly indistinguishable; Table 1 reports the total variation distances, which are small. These observations indicate that the proposed schemes yield statistically consistent long-time behavior and can recover long-time statistics of the 2D NSE [3, 4, 19]. The fat tail in the PDF is consistent with the bursting and intermittent behavior observed in Figure 4.

Table 1: Total variation distance between enstrophy distributions obtained by ETD-mr-SAV-MS2o, ETD-mr-SAV-MS12 for  $\nu = 1/40$  and  $m = 4$ .

$L^2$ Norm of Vorticity	Total Variation Distance	Relative $L^1$ Error
$\ \omega\  < 17.5$	0.006926	0.481124%
$\ \omega\  \geq 17.5$	0.014793	1.593388%
$-\infty \leq \ \omega\  \leq \infty$	0.021715	2.074374%

These results collectively validate the effectiveness of the ETD-mr-SAV-MS12 scheme: it provides automatic short-time error control while maintaining long-time stability, and it recovers long-time statistics with significantly improved efficiency.

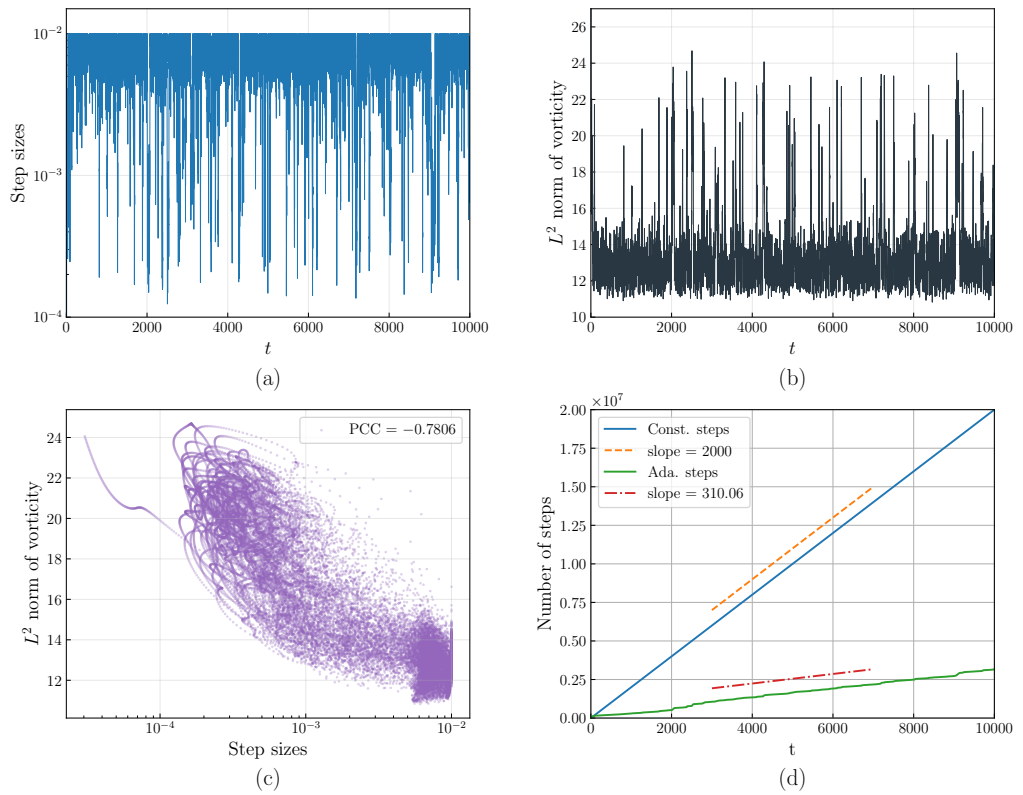


Figure 6: (a) Adaptive time step sizes as a function of time. (b) Enstrophy ( $L^2$  norm of vorticity) as a function of time. (c) Rate of change of enstrophy as a function of time. (d) Correlation between step sizes and enstrophy ( $PCC = -0.7806$ ). (e) Number of steps over time for constant steps and adaptive steps.

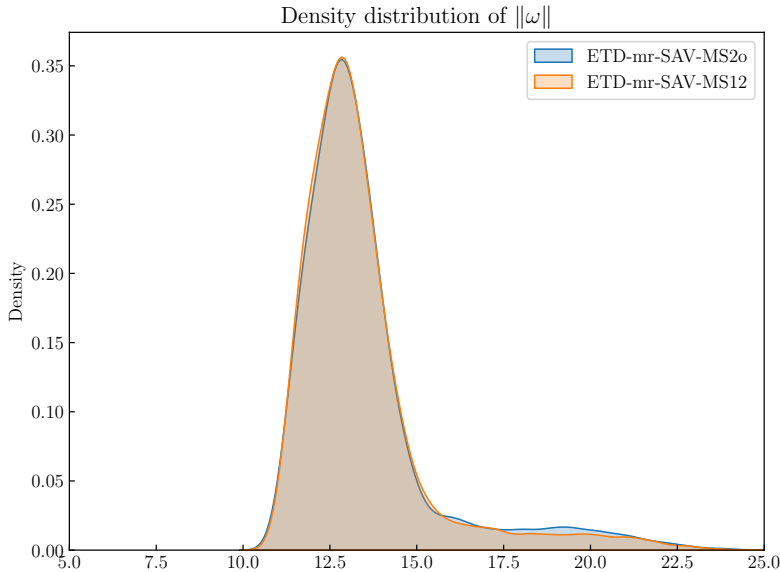


Figure 7: Probability density functions of enstrophy obtained by ETD-mr-SAV-MS2o and ETD-mr-SAV-MS12 for  $\nu = 1/40$  and  $m = 4$ .

## 6. Conclusion

We have developed an efficient, unconditionally long-time stable, variable-step, second-order exponential time-differencing (ETD) scheme for the incompressible Navier–Stokes equations in periodic domains, together with two small variants. The proposed methods are long-time stable in the sense that the numerical solutions admit uniform-in-time bounds in the space  $L^\infty(0, \infty; L^2)$  under general external forcing, independently of the time-step size and the viscosity parameter. This fundamental stability property provides a solid foundation for the accurate approximation of long-time statistical quantities and asymptotic regimes.

Our approach integrates a recently developed mean-reverting scalar auxiliary variable (mr-SAV) formulation with a dynamic second-order correction strategy and multistep ETD techniques. This combination plays a central role in ensuring unconditional long-time stability while maintaining second-order temporal accuracy under variable step sizes. The resulting schemes are fully linear in the fluid variables and remain solvable for arbitrary parameter values.

From a computational perspective, the proposed methods are highly efficient, requiring only two Stokes solves and the solution of a single scalar cubic algebraic equation at each time step. An embedded adaptive time-stepping strategy, based on a first-order companion scheme, has also been developed to automatically adjust the time-step size in response to the evolving dynamics, thereby improving efficiency without sacrificing stability.

The numerical experiments presented in this work confirm the theoretical analysis. In particular, they demonstrate the expected second-order temporal convergence, unconditional long-time stability under variable time stepping. Moreover, the adaptive strategy effectively balances accuracy and efficiency, leading to substantial computational savings in problems with multiscale temporal behavior.

While the present results are encouraging, several important directions merit further investigation. These include the development of rigorous convergence analyses under minimal regularity assumptions, systematic studies of the convergence of long-time statistical properties, the construction of higher-order long-time stable variable-step schemes, and extensions to non-periodic boundary conditions. In addition, applying the proposed framework to more complex fluid models, such as the Boussinesq equations for thermal convection and phase-field-based two-phase flow systems, represents a promising avenue for future research.

The unconditional long-time stability and statistical consistency of the proposed ETD-mr-SAV framework also make it well suited for integration with modern data-driven and machine learning methodologies in fluid dynamics. In particular, reliable numerical approximation of invariant measures, long-time averages, and intermittent bursting dynamics is essential for training and validating reduced-order models, operator learning frameworks, and physics-informed neural networks. Many existing learning-based approaches suffer from accumulated numerical drift and distorted long-time statistics due to deficiencies in the underlying solvers. By preserving uniform-in-time energy bounds under variable step sizes, the present schemes provide a robust computational backbone for generating high-fidelity training data over long time horizons.

Moreover, the ability of the proposed methods to efficiently resolve intermittent and extreme events enables systematic investigation of rare-event dynamics in turbulent and

transitional flows. Such events play a critical role in climate modeling, geophysical flows, and engineering applications, yet remain challenging to predict using purely data-driven techniques. Coupling the present long-time stable solvers with machine learning tools for reduced-order modeling, uncertainty quantification, and rare-event prediction offers a promising avenue for improving both physical understanding and predictive capability. In particular, the adaptive time-stepping strategy facilitates targeted resolution of rapid transients and extreme fluctuations, which is advantageous for learning precursors and probabilistic forecasts of rare events.

These directions suggest that structure-preserving ETD-mr-SAV methods may serve as a foundation for hybrid physics–machine learning frameworks aimed at long-time forecasting, statistical inference, and data-driven discovery in complex fluid systems.

### **Acknowledgment**

This work is supported in part by NSFC12271237. The second author acknowledges helpful conversation with Professors Wenbin Chen and Qiang Du.

### **Declarations**

The authors declare that they have no known competing financial interests or personal relationships that could have appeared to influence the work reported in this paper.

### **References**

- [1] U. Frisch, A. N. Kolmogorov, *Turbulence: the legacy of A. N. Kolmogorov*, Cambridge University Press, 1995.
- [2] P. Constantin, C. Foias, *Navier-Stokes equations*, University of Chicago Press, 1988.
- [3] C. Foias, O. Manley, R. Rosa, R. Temam, *Navier-Stokes equations and turbulence*, Vol. 83, Cambridge University Press, 2001.
- [4] A. Majda, X. Wang, *Nonlinear dynamics and statistical theories for basic geophysical flows*, Cambridge University Press, 2006.

[5] R. Temam, Infinite-dimensional dynamical systems in mechanics and physics, Vol. 68, Springer-Verlag, New York, 1988.

[6] J. G. Heywood, R. Rannacher, Finite-element approximation of the nonstationary Navier–Stokes problem. Part IV: error analysis for second-order time discretization, *SIAM Journal on Numerical Analysis* 27 (2) (1990) 353–384. doi:10.1137/0727022.

[7] C. Lubich, A. Ostermann, Runge–Kutta time discretization of reaction-diffusion and Navier–Stokes equations: nonsmooth-data error estimates and applications to long-time behaviour, *Applied Numerical Mathematics* 22 (1-3) (1996) 279–292. doi:10.1016/S0168-9274(96)00038-4.

[8] F. Tone, D. Wirosoetisno, On the long-time stability of the implicit Euler scheme for the two-dimensional Navier–Stokes equations, *SIAM Journal on Numerical Analysis* 44 (1) (2006) 29–40. doi:10.1137/040618527.

[9] F. Tone, On the long-time stability of the Crank–Nicolson scheme for the 2D Navier–Stokes equations, *Numerical Methods for Partial Differential Equations: An International Journal* 23 (5) (2007) 1235–1248. doi:10.1002/num.20219.

[10] T. Geveci, On the convergence of a time discretization scheme for the Navier–Stokes equations, *Mathematics of Computation* 53 (187) (1989) 43–53. doi:10.1090/S0025-5718-1989-0969488-5.

[11] J. Simo, F. Armero, Unconditional stability and long-term behavior of transient algorithms for the incompressible Navier–Stokes and Euler equations, *Computer Methods in Applied Mechanics and Engineering* 111 (1-2) (1994) 111–154. doi:10.1016/0045-7825(94)90042-6.

[12] N. Ju, On the global stability of a temporal discretization scheme for the Navier–Stokes equations, *IMA Journal of Numerical Analysis* 22 (4) (2002) 577–597. doi:10.1093/imanum/22.4.577.

[13] T. Heister, M. A. Olshanskii, L. G. Rebholz, Unconditional long-time stability of a velocity–vorticity method for the 2D Navier–Stokes equations, *Numerische Mathematik* 135 (1) (2017) 143–167. doi:10.1007/s00211-016-0794-1.

- [14] A. T. Hill, E. Süli, Approximation of the global attractor for the incompressible Navier–Stokes equations, *IMA Journal of Numerical Analysis* 20 (4) (2000) 633–667. [doi:10.1093/imanum/20.4.633](https://doi.org/10.1093/imanum/20.4.633).
- [15] L. Rebholz, F. Tone, Long-time  $H^1$ -stability of BDF2 time stepping for 2D Navier–Stokes equations, *Applied Mathematics Letters* 141 (2023) 108624. [doi:10.1016/j.aml.2023.108624](https://doi.org/10.1016/j.aml.2023.108624).
- [16] A. Contri, B. Kovács, A. Massing, Error analysis of BDF 1–6 time-stepping methods for the transient Stokes problem: velocity and pressure estimates, *SIAM Journal on Numerical Analysis* 63 (4) (2025) 1586–1616. [doi:10.1137/23M1606800](https://doi.org/10.1137/23M1606800).
- [17] B. García-Archilla, V. John, J. Novo, Error analysis of BDF schemes for the evolutionary incompressible Navier–Stokes equations, arXiv preprint arXiv:2506.16917 (2025).
- [18] S. Gottlieb, F. Tone, C. Wang, X. Wang, D. Wirosoetisno, Long time stability of a classical efficient scheme for two-dimensional Navier–Stokes equations, *SIAM Journal on Numerical Analysis* 50 (1) (2012) 126–150. [doi:10.1137/110834901](https://doi.org/10.1137/110834901).
- [19] X. Wang, An efficient second order in time scheme for approximating long time statistical properties of the two dimensional Navier–Stokes equations, *Numerische Mathematik* 121 (4) (2012) 753–779. [doi:10.1007/s00211-012-0450-3](https://doi.org/10.1007/s00211-012-0450-3).
- [20] K. Cheng, C. Wang, Long time stability of high order multistep numerical schemes for two-dimensional incompressible Navier–Stokes equations, *SIAM Journal on Numerical Analysis* 54 (5) (2016) 3123–3144. [doi:10.1137/16M1061588](https://doi.org/10.1137/16M1061588).
- [21] Q. Du, W.-x. Zhu, Stability analysis and application of the exponential time differencing schemes, *Journal of Computational Mathematics* (2004) 200–209.
- [22] Q. Du, W. Zhu, Analysis and applications of the exponential time differencing schemes and their contour integration modifications, *BIT Numerical Mathematics* 45 (2) (2005) 307–328.

- [23] L. Ju, X. Li, Z. Qiao, H. Zhang, Energy stability and error estimates of exponential time differencing schemes for the epitaxial growth model without slope selection, *Mathematics of Computation* 87 (312) (2018) 1859–1885.
- [24] Q. Du, L. Ju, X. Li, Z. Qiao, Maximum bound principles for a class of semilinear parabolic equations and exponential time-differencing schemes, *SIAM Review* 63 (2) (2021) 317–359.
- [25] H. Wang, J. Sun, H. Zhang, X. Qian, A novel up to fourth-order equilibria-preserving and energy-stable exponential Runge–Kutta framework for gradient flows, *CSIAM Transactions on Applied Mathematics* 6 (1) (2025) 106–147.
- [26] W. Chen, S. Wang, X. Wang, Energy Stable Arbitrary Order ETD-MS Method for Gradient Flows with Lipschitz Nonlinearity, *CSIAM Transactions on Applied Mathematics* 2 (3) (2021) 460–483.
- [27] Z. Fu, J. Yang, Energy-decreasing exponential time differencing Runge–Kutta methods for phase-field models, *Journal of Computational Physics* 454 (2022) 110943.
- [28] Z. Fu, J. Shen, J. Yang, Higher-order energy-decreasing exponential time differencing Runge–Kutta methods for gradient flows, *Science China Mathematics* 68 (7) (2025) 1727–1746.
- [29] W. Chen, Z. F. Fu, S. Wang, X. Wang, Convergence of long-time stable variable-step arbitrary order ETD-MS scheme for gradient flows with Lipschitz nonlinearity, arxiv preprint arXiv.2512.01601 (2025). doi:<https://doi.org/10.48550/arXiv.2512.01601>.
- [30] L. Zhang, Un schéma de semi-discrétisation en temps pour des systèmes différentiels discrétisés en espace par la méthode de fourier: résolution numérique des équations de navier-stokes stationnaires par la méthode multigrille, Ph.D. thesis, Paris 11 (1987).
- [31] R. S. Rogallo, An ILLIAC program for the numerical simulation of homogeneous incompressible turbulence, Tech. rep., NASA TM-73203 (1977).

- [32] G. L. Kooij, M. A. Botchev, B. J. Geurts, An exponential time integrator for the incompressible Navier–Stokes equation, *SIAM Journal on Scientific Computing* 40 (3) (2018) B684–B705. [doi:10.1137/17M1121950](https://doi.org/10.1137/17M1121950).
- [33] S. Li, Z. J. Wang, L. Ju, L. Luo, Fast time integration of Navier–Stokes equations with an exponential-integrator scheme, in: 2018 AIAA Aerospace Sciences Meeting, 2018, p. 0369. [doi:10.2514/6.2018-0369](https://doi.org/10.2514/6.2018-0369).
- [34] S. Li, L. Ju, H. Si, Adaptive exponential time integration of the Navier–Stokes equations, in: AIAA Scitech 2020 Forum, 2020, p. 2033. [doi:10.2514/6.2020-2033](https://doi.org/10.2514/6.2020-2033).
- [35] J. Shen, J. Xu, J. Yang, The scalar auxiliary variable (SAV) approach for gradient flows, *Journal of Computational Physics* 353 (2018) 407–416. [doi:10.1016/j.jcp.2017.10.021](https://doi.org/10.1016/j.jcp.2017.10.021).
- [36] J. Shen, J. Xu, J. Yang, A new class of efficient and robust energy stable schemes for gradient flows, *SIAM Review* 61 (3) (2019) 474–506. [doi:10.1137/17M1150153](https://doi.org/10.1137/17M1150153).
- [37] G. Akrivis, B. Li, D. Li, Energy-decaying extrapolated RK–SAV methods for the Allen–Cahn and Cahn–Hilliard equations, *SIAM Journal on Scientific Computing* 41 (6) (2019) A3703–A3727. [doi:10.1137/19M1264412](https://doi.org/10.1137/19M1264412).
- [38] L. Lin, Z. Yang, S. Dong, Numerical approximation of incompressible Navier–Stokes equations based on an auxiliary energy variable, *Journal of Computational Physics* 388 (2019) 1–22. [doi:10.1016/j.jcp.2019.03.012](https://doi.org/10.1016/j.jcp.2019.03.012).
- [39] L. Lin, N. Ni, Z. Yang, S. Dong, An energy-stable scheme for incompressible Navier–Stokes equations with periodically updated coefficient matrix, *Journal of Computational Physics* 418 (2020) 109624.
- [40] F. Huang, J. Shen, Stability and error analysis of a second-order consistent splitting scheme for the Navier–Stokes equations, *SIAM Journal on Numerical Analysis* 61 (5) (2023) 2408–2433. [doi:10.1137/23M1556022](https://doi.org/10.1137/23M1556022).
- [41] F. Huang, J. Shen, Stability and error analysis of a new class of higher-order consistent splitting schemes for the Navier–Stokes equations, *Mathematics of Computation* (2025). [doi:10.1090/mcom/4132](https://doi.org/10.1090/mcom/4132).

- [42] Y. Di, Y. Ma, J. Shen, J. Zhang, A variable time-step IMEX-BDF2 SAV scheme and its sharp error estimate for the Navier–Stokes equations, *ESAIM: Mathematical Modelling and Numerical Analysis* 57 (3) (2023) 1143–1170.
- [43] B. Ji, H. Liao, A unified  $L^2$  norm error analysis of SAV-BDF schemes for the incompressible Navier–Stokes equations, *Journal of Scientific Computing* 100 (1) (2024) 5.
- [44] S. Zeng, Z. Xie, X. Yang, J. Wang, Fully discrete, decoupled and energy-stable Fourier-Spectral numerical scheme for the nonlocal Cahn–Hilliard equation coupled with Navier–Stokes/Darcy flow regime of two-phase incompressible flows, *Computer Methods in Applied Mechanics and Engineering* 415 (2023) 116289.
- [45] G. D. Zhang, X. He, X. Yang, A unified framework of the SAV-ZEC method for a mass-conserved Allen–Cahn type two-phase ferrofluid flow model, *SIAM Journal on Scientific Computing* 46 (2) (2024) B77–B106. [doi:10.1137/23M1569125](https://doi.org/10.1137/23M1569125).
- [46] G.-D. Zhang, S. Zhou, Y. Huang, X. He, X. Yang, A diffuse interface model and fully decoupled, energy-stable scheme for the two-phase ferrofluid flows in porous media, *Journal of Computational Physics* (2025) 114561.
- [47] D. Han, X. Wang, A highly efficient second-order accurate long-time dynamics preserving scheme for some geophysical fluid models, *arXiv preprint arXiv:2510.05360* (2025).
- [48] J. Coleman, D. Han, X. Wang, An efficient scheme for approximating long-time dynamics of a class of non-linear models, *Communications in Information and Systems* 25 (2) (2025) 273–299.
- [49] D. Hou, Z. Qiao, An implicit–explicit second-order BDF numerical scheme with variable steps for gradient flows, *Journal of Scientific Computing* 94 (2) (2023) 39.
- [50] F. Huang, J. Shen, A new class of implicit–explicit BDFk SAV schemes for general dissipative systems and their error analysis, *Computer Methods in Applied Mechanics and Engineering* 392 (2022) 114718. [doi:10.1016/j.cma.2022.114718](https://doi.org/10.1016/j.cma.2022.114718).

- [51] X. Yang, A new efficient fully-decoupled and second-order time-accurate scheme for Cahn–Hilliard phase-field model of three-phase incompressible flow, *Computer Methods in Applied Mechanics and Engineering* 376 (2021) 113589. [doi:10.1016/j.cma.2020.113589](https://doi.org/10.1016/j.cma.2020.113589).
- [52] X. Yang, A novel fully-decoupled, second-order and energy stable numerical scheme of the conserved Allen–Cahn type flow-coupled binary surfactant model, *Computer Methods in Applied Mechanics and Engineering* 373 (2021) 113502. [doi:10.1016/j.cma.2020.113502](https://doi.org/10.1016/j.cma.2020.113502).
- [53] X. Li, J. Shen, Z. Liu, New SAV-pressure correction methods for the Navier-Stokes equations: stability and error analysis, *Mathematics of Computation* 91 (333) (2022) 141–167. [doi:10.1090/mcom/3651](https://doi.org/10.1090/mcom/3651).
- [54] E. Hairer, G. Wanner, S. P. Nørsett, *Solving ordinary differential equations I: Non-stiff problems*, Springer, 1993.
- [55] W. Chen, X. Wang, Y. Yan, Z. Zhang, A second order BDF numerical scheme with variable steps for the Cahn–Hilliard equation, *SIAM Journal on Numerical Analysis* 57 (1) (2019) 495–525. [doi:10.1137/18M1206084](https://doi.org/10.1137/18M1206084).
- [56] A. K. Kassam, L. N. Trefethen, Fourth-order time-stepping for stiff PDEs, *SIAM Journal on Scientific Computing* 26 (4) (2005) 1214–1233. [doi:10.1137/S1064827502410633](https://doi.org/10.1137/S1064827502410633).
- [57] D. Armbruster, B. Nicolaenko, N. Smaoui, P. Chossat, Symmetries and dynamics for 2-D Navier-Stokes flow, *Physica D: Nonlinear Phenomena* 95 (1) (1996) 81–93. [doi:10.1016/0167-2789\(96\)00006-1](https://doi.org/10.1016/0167-2789(96)00006-1).